In vivo monitoring of protein-bound and free NADH during ischemia by nonlinear spectral imaging microscopy

Jonathan A. Palero,[1,2] Arjen N. Bader,[1] Henriëtte S. de Bruijn,[3] Angélique van der Ploeg van den Heuvel,[3] Henricus J. C. M. Sterenborg,[3] and Hans C. Gerritsen[1,*]

[1] *Molecular BioPhysics, Utrecht University, 3584 CC Utrecht, The Netherlands*
[2]*Currently with ICFO-Institut de Ciències Fotòniques, Mediterranean Technology Park, 08860 Castelldefels (Barcelona), Spain*
[3]*Department of Radiation Oncology,Center of Optical Diagnostics and Therapy, Erasmus Medical Center, 3008 AE Rotterdam, The Netherlands*
[*]H.C.Gerritsen@uu.nl

Abstract: Nonlinear spectral imaging microscopy (NSIM) allows simultaneous morphological and spectroscopic investigation of intercellular events within living animals. In this study we used NSIM for *in vivo* time-lapse in-depth spectral imaging and monitoring of protein-bound and free reduced nicotinamide adenine dinucleotide (NADH) in mouse keratinocytes following total acute ischemia for 3.3 h at ~3 min time intervals. The high spectral resolution of NSIM images allows discrimination between the two-photon excited fluorescence emission of protein-bound and free NAD(P)H by applying linear spectral unmixing to the spectral image data. Results reveal the difference in the dynamic response between protein-bound and free NAD(P)H to ischemia-induced hypoxia/anoxia. Our results dem–onstrate the capability of nonlinear spectral imaging microscopy in unraveling dynamic cellular metabolic events within living animals for long periods of time.

OCIS codes: (110.4234) Multispectral and hyperspectral imaging; (170.1470) Blood or tissue constituent monitoring; (180.2520) Fluorescence microscopy; (190.4180) Multiphoton processes.

References and links

1. B. Chance, P. Cohen, F. Jobsis, and B. Schoener, "Intracellular oxidation-reduction states in vivo," Science **137**(3529), 499–508 (1962).
2. W. R. Zipfel, R. M. Williams, R. Christie, A. Y. Nikitin, B. T. Hyman, and W. W. Webb, "Live tissue intrinsic emission microscopy using multiphoton-excited native fluorescence and second harmonic generation," Proc. Natl. Acad. Sci. U.S.A. **100**(12), 7075–7080 (2003).
3. J. A. Palero, H. S. de Bruijn, A. van der Ploeg van den Heuvel, H. J. Sterenborg, and H. C. Gerritsen, "Spectrally resolved multiphoton imaging of in vivo and excised mouse skin tissues," Biophys. J. **93**(3), 992–1007 (2007).
4. J. A. Palero, H. S. de Bruijn, A. van der Ploeg-van den Heuvel, H. J. Sterenborg, and H. C. Gerritsen, "In vivo nonlinear spectral imaging in mouse skin," Opt. Express **14**(10), 4395–4402 (2006).
5. E. C. Rothstein, S. Carroll, C. A. Combs, P. D. Jobsis, and R. S. Balaban, "Skeletal muscle NAD(P)H two-photon fluorescence microscopy in vivo: topology and optical inner filters," Biophys. J. **88**(3), 2165–2176 (2005).
6. M. C. Skala, K. M. Riching, A. Gendron-Fitzpatrick, J. Eickhoff, K. W. Eliceiri, J. G. White, and N. Ramanujam, "In vivo multiphoton microscopy of NADH and FAD redox states, fluorescence lifetimes, and cellular morphology in precancerous epithelia," Proc. Natl. Acad. Sci. U.S.A. **104**(49), 19494–19499 (2007).
7. H. D. Vishwasrao, A. A. Heikal, K. A. Kasischke, and W. W. Webb, "Conformational dependence of intracellular NADH on metabolic state revealed by associated fluorescence anisotropy," J. Biol. Chem. **280**(26), 25119–25126 (2005).
8. V. K. Ramanujan, J. A. Jo, G. Cantu, and B. A. Herman, "Spatially resolved fluorescence lifetime mapping of enzyme kinetics in living cells," J. Microsc. **230**(3), 329–338 (2008).
9. V. V. Ghukasyan and F.-J. Kao, "Monitoring cellular metabolism with fluorescence lifetime of reduced nicotinamide adenine dinucleotide," J. Phys. Chem. C **113**(27), 11532–11540 (2009).

10. M. C. Skala, K. M. Riching, D. K. Bird, A. Gendron-Fitzpatrick, J. Eickhoff, K. W. Eliceiri, P. J. Keely, and N. Ramanujam, "In vivo multiphoton fluorescence lifetime imaging of protein-bound and free nicotinamide adenine dinucleotide in normal and precancerous epithelia," J. Biomed. Opt. **12**(2), 024014 (2007).
11. Q. Yu and A. A. Heikal, "Two-photon autofluorescence dynamics imaging reveals sensitivity of intracellular NADH concentration and conformation to cell physiology at the single-cell level," J. Photochem. Photobiol. B **95**(1), 46–57 (2009).
12. D. Li, W. Zheng, and J. Y. Qu, "Time-resolved spectroscopic imaging reveals the fundamentals of cellular NADH fluorescence," Opt. Lett. **33**(20), 2365–2367 (2008).
13. D. K. Bird, L. Yan, K. M. Vrotsos, K. W. Eliceiri, E. M. Vaughan, P. J. Keely, J. G. White, and N. Ramanujam, "Metabolic mapping of MCF10A human breast cells via multiphoton fluorescence lifetime imaging of the coenzyme NADH," Cancer Res. **65**(19), 8766–8773 (2005).
14. J. A. Palero, G. Latouche, H. S. de Bruijn, A. van der Ploeg van den Heuvel, H. J. Sterenborg, and H. C. Gerritsen, "Design and implementation of a sensitive high-resolution nonlinear spectral imaging microscope," J. Biomed. Opt. **13**(4), 044019 (2008).
15. J. Palero, "Nonlinear spectral imaging microscopy," Imaging Microsc. **11**(1), 22–25 (2009).
16. P. L. T. M. Frederix, M. A. H. Asselbergs, W. G. J. H. M. Van Sark, D. J. Van den Heuvel, W. Hamelink, E. L. de Beer, and H. C. Gerritsen, "High sensitivity spectrograph for use in fluorescence microscopy," Appl. Spectrosc. **55**(8), 1005–1012 (2001).
17. A. Esposito, A. N. Bader, S. C. Schlachter, D. J. van den Heuvel, G. S. K. Schierle, A. R. Venkitaraman, C. F. Kaminski, and H. C. Gerritsen, "Design and application of a confocal microscope for spectrally resolved anisotropy imaging," Opt. Express **19**(3), 2546–2555 (2011).
18. J. A. Palero, H. S. de Bruijn, A. van der Ploeg van den Heuvel, H. J. Sterenborg, H. van Weelden, and H. C. Gerritsen, "In vivo nonlinear spectral imaging microscopy of visible and ultraviolet irradiated hairless mouse skin tissues," Photochem. Photobiol. Sci. **7**(11), 1422–1425 (2008).
19. A. N. Bader, A.-M. Pena, C. Johan van Voskuilen, J. A. Palero, F. Leroy, A. Colonna, and H. C. Gerritsen, "Fast nonlinear spectral microscopy of in vivo human skin," Biomed. Opt. Express **2**(2), 365–373 (2011).
20. G. Weagle, P. E. Paterson, J. Kennedy, and R. Pottier, "The nature of the chromophore responsible for naturally occurring fluorescence in mouse skin," J. Photochem. Photobiol. B **2**(3), 313–320 (1988).
21. A. Amelink and H. J. Sterenborg, "Measurement of the local optical properties of turbid media by differential path-length spectroscopy," Appl. Opt. **43**(15), 3048–3054 (2004).
22. J. A. Gardecki and M. Maroncelli, "Set of secondary emission standards for calibration of the spectral responsivity in emission spectroscopy," Appl. Spectrosc. **52**(9), 1179–1189 (1998).
23. J. R. Lakowicz, H. Szmacinski, K. Nowaczyk, and M. L. Johnson, "Fluorescence lifetime imaging of free and protein-bound NADH," Proc. Natl. Acad. Sci. U.S.A. **89**(4), 1271–1275 (1992).
24. R. Richards-Kortum and E. Sevick-Muraca, "Quantitative optical spectroscopy for tissue diagnosis," Annu. Rev. Phys. Chem. **47**(1), 555–606 (1996).
25. K. Blinova, R. L. Levine, E. S. Boja, G. L. Griffiths, Z. D. Shi, B. Ruddy, and R. S. Balaban, "Mitochondrial NADH fluorescence is enhanced by complex I binding," Biochemistry **47**(36), 9636–9645 (2008).
26. N. D. Evans, L. Gnudi, O. J. Rolinski, D. J. Birch, and J. C. Pickup, "Glucose-dependent changes in NAD(P)H-related fluorescence lifetime of adipocytes and fibroblasts in vitro: potential for non-invasive glucose sensing in diabetes mellitus," J. Photochem. Photobiol. B **80**(2), 122–129 (2005).
27. G. Ronquist, A. Andersson, N. Bendsoe, and B. Falck, "Human epidermal energy metabolism is functionally anaerobic," Exp. Dermatol. **12**(5), 572–579 (2003).
28. M. Stücker, A. Struk, P. Altmeyer, M. Herde, H. Baumgärtl, and D. W. Lübbers, "The cutaneous uptake of atmospheric oxygen contributes significantly to the oxygen supply of human dermis and epidermis," J. Physiol. **538**(3), 985–994 (2002).
29. T. Galeotti, G. D. van Rossum, D. H. Mayer, and B. Chance, "On the fluorescence of NAD(P)H in whole-cell preparations of tumours and normal tissues," Eur. J. Biochem. **17**(3), 485–496 (1970).
30. Z. Abramovic, M. Sentjurc, J. Kristl, N. Khan, H. Hou, and H. M. Swartz, "Influence of different anesthetics on skin oxygenation studied by electron paramagnetic resonance in vivo," Skin Pharmacol. Physiol. **20**(2), 77–84 (2007).

1. Introduction

The autofluorescence of reduced nicotinamide adenine dinucleotides (NADH) can reveal the metabolic state of a cell. For decades now, NADH, the principal electron donor in glycolytic and oxidative energy metabolism, has been used as a convenient noninvasive probe of cellular metabolic state [1]. Although it exists in an oxidized (NAD$^+$) and a reduced (NADH) form, only NADH is intrinsically fluorescent, whereas its oxidized product (NAD$^+$) is not. Chance et al. took advantage of this phenomenon and demonstrated that microfluorometry of NADH provides a means to probe the oxidation-reduction state of cells and tissues [1]. This pioneering work opened the door to more studies that utilized probing NADH fluorescence to reveal the metabolic activity within the cell. The emergence of nonlinear-excited fluorescence microscopy paved the way to a new era of cellular imaging in thick samples as well as living

animals [2–4] leading to key advancement in metabolic studies of cells from isolated samples to *in vivo* conditions [5,6].

In recent years, there have been a growing number of reports on studies of NADH that were largely focused on time-resolved fluorescence and anisotropy measurements demonstrating capability to discriminate protein-bound and free NADH in the intracellular environment [7–13]. In principle, discrimination between protein-bound and free NADH is also achievable by fluorescence emission spectroscopy. However, high spectral resolution measurement is necessary to discriminate the two emission bands due to close proximity of their spectral peaks ($\lambda_{boundNADH} \approx 445$ nm; $\lambda_{freeNADH} \approx 460$ nm) and their large spectral overlap ($\Delta\lambda_{boundNADH} \approx \Delta\lambda_{freeNADH} \approx 90$ nm). To address this issue, we developed high-resolution spatial and spectral nonlinear spectral imaging microscopy (NSIM) [14,15]. This technique combines spectral imaging microscopy [16,17] with nonlinear microscopy (multiphoton-excited fluorescence and second harmonic generation) to obtain spectrally-resolved optical sections of living tissues. Further implementation of linear spectral unmixing showed the potential of NSIM in obtaining biochemical information from in-vivo spectral images of mouse [3,4,18] and human skin [19]. In this study, we demonstrate the capability of NSIM to discriminate in-vivo protein-bound and free NADH in mouse keratinocytes following total acute ischemia. Moreover, the use of low excitation power levels and the inherent localization of nonlinear excitation allowed us to acquire spectral images for up to 3.3 hr with minimal photobleaching.

2. Materials and method

2.1. Animal model

The Committee on Animal Research of the Erasmus University Rotterdam approved the experimental protocol. The skin of two female inbred albino hairless mice (SKH1 HR, Charles River, Someren, The Netherlands) was used *in vivo*. The mice were fed on a diet free of chlorophyll (Hope Farms BV, Woerden, The Netherlands) for a minimum of 2 weeks before starting the experiments to remove the autofluorescence emission from mouse skin centered at 675 nm attributed to pheophorbide-a [20]. The mice were placed on a home-made temperature-controlled microscope stage. During pre-ischemia imaging, the mice were anaesthetized using Ketamine (80mg/kg, Janssen Pharmaceutica, Tilburg, The Netherlands) and Rompun (10mg/kg Janssen Pharmaceutica, Tilburg, The Netherlands), both were administered intraperitoneally. Acute ischemia was induced by euthanizing the anaesthetized animal. Blood oxygenation in the mouse tongue was measured using differential path-length spectroscopy [21]. Blood oxygenation levels of ~50% were found in the anaesthetized mouse; this value dropped to 0% immediately (< 1 min) after administration of the euthanasia solution. All experiments were limited to four hours after anesthesia administration.

2.2. Nonlinear spectral imaging microscope

The basic NSIM setup used for detecting autofluorescence signal from *in vivo* keratinocytes was similar to that described previously [14]. A diagram of the experimental setup is shown in Fig. 1. The excitation light source (765 nm) was a mode-locked titanium:sapphire (Ti:Sa) laser (Tsunami, Spectra-Physics, Sunnyvale, CA), pumped by a 5W neodymium yttrium vanadate (Nd:YVO$_4$) laser (Millennia, Spectra-Physics, Sunnyvale, CA). The laser light was scanned using a galvanometer mirror scanner (040EF, LSK, Stallikon, Switzerland). In addition to the beam-scanning mechanism, the microscope was also equipped with an XYZ piezo translation (sample) stage (Physik Instrumente, Karlsruhe/Palmbach, Germany). The laser light was focused by an objective lens on the sample and the fluorescence emission was collected by the same objective lens. The results reported here were acquired in the inverted geometry using an infinity-corrected oil-immersion objective lens (60× and NA = 1.40, Nikon, Japan).

The emission passed through a dichroic mirror and was filtered by a set of short-pass Schott® optical glass filters (total thickness = 7 mm; BG-40, Schott, Mainz, Germany). The filtered light was dispersed by two prisms and focused on the charge-coupled device (CCD)

camera by a UV-VIS-IR achromat (diameter = 40 mm, focal length = 160 mm; Bernhard Halle Nachfl., Berlin, Germany). The spectrograph was equipped with a thermoelectrically cooled, back-illuminated CCD camera (Princeton Instruments, Spec-10:2KBUV, 16-bit, ST-133 controller, typical read noise 3 e⁻ rms at 100-kHz digitization). In our experiments, the exposure time was limited to 2.1 ms per pixel and employed excitation powers of less than 5 mW. Photobleaching was observed to be minimal at this low power level. Based on the recorded images prior to the administration of euthanasia solution, we estimated a fluorescence (bleaching) decay rate ($1/e$) of 2.5×10^{-3}/frame at 2 min/frame. Data processing and visualization were carried out using a program (SpecView) written in IDL 6.0 (Research Systems Inc., Boulder, CO).
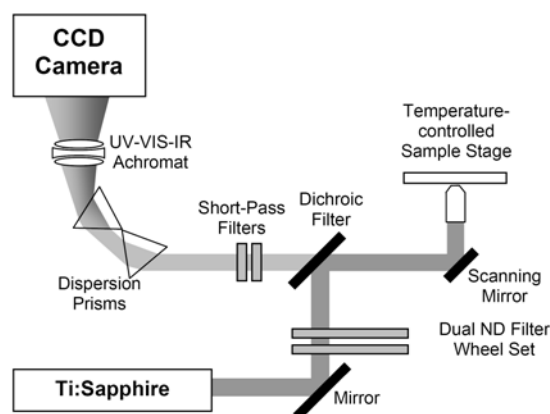

Fig. 1. Schematic diagram of the spectral imaging setup. The intrinsic emission of a sample is epi-detected without a pinhole. The signal is spectrally dispersed by two prisms, focused with an achromat, and detected with a back-illuminated CCD array.

Wavelength and instrument spectral response calibration of the instrument was carried out to ensure accurate spectral measurements. A white light source and a calibrated monochromator were used to calibrate the instrument wavelength and the calibration accuracy was better than 0.5 nm over the whole wavelength range. The spectral response correction was calculated by measuring the spectra of two standard fluorophores: tryptophan in water and quinine sulfate in perchloric acid [22].

2.3. Visualization and analysis of spectral image data

The recorded spectral image data were converted to RGB images for visualization using a program written in IDL 6.0 (Research Systems Inc., Boulder, CO) as described in detail previously [4]. Briefly, the conversion procedure involves down sampling the 100-channel (wavelength) spectral image to a 3-channel (RGB) color image. The full spectral image data set were analyzed using a separate program written in IDL 6.0. Pixel-averaged spectra of selected regions-of-interest (ROIs) were obtained for spectral analysis depicted in Fig. 2 (*yellow dashed box*). The basis of selecting an area as an alternative to using the whole image is to ensure that only keratinocytes from a single tissue layer, in our case mainly the stratum basale were analyzed.

Linear spectral unmixing analysis was performed by means of iterative linear least squares fitting procedure (Gaussian multi-peaks, Origin® 6.1, OriginLab Corporation, Northampton, MA, USA). Three Gaussian curves were fitted globally using the difference spectra (see Fig. 3 D) from all time points relative to the time before acute ischemia was induced, thus removing static components from the analyses. The shared parameters for this procedure were the spectral peak positions and spectral widths while the amplitudes were allowed to vary. All fitting procedures were carried out in the wavenumber space. The global fit yielded the time-varying amplitudes of the spectral components attributed to the autofluorescence of protein-bound and free NADH and flavins as depicted in Fig. 4 A.

3. Results

3.1. Cellular autofluorescence modification following total acute ischemia

The capability of nonlinear microscopy to produce optical sections through thick tissues allowed us to record spectral images of living cells inside the epidermis. In addition, the high sensitivity of the spectral imaging system across a broad spectral range (350 nm to 600 nm) permitted acquisition of autofluorescence spectral images with relatively high signal-to-noise ratio (SNR) using low excitation power levels, typically around 5 mW [14]. Long-term *in vivo* imaging of cells within tissues using the present setup is thus achieved with minimal photobleaching and low phototoxicity.
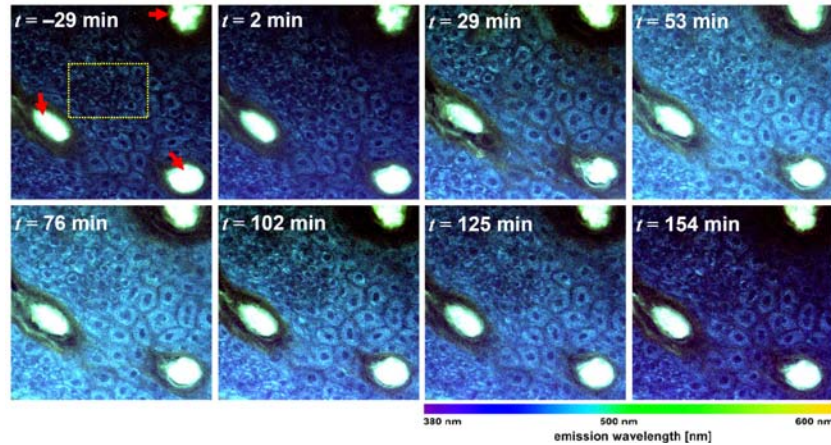

Fig. 2. Representative time-lapse RGB spectral images of mouse keratinocytes *in vivo* before (t < 0 min) and during (t > 0 min) ischemia showing increase and decrease in autofluorescence (AF). Red arrows: hair follicles. Colors represent emission wavelength as indicated in color bar. All images are 224 × 224 pixels, 100 μm × 100 μm.

Time series of spectrally-resolved nonlinear-excited fluorescence optical sections were recorded from the skin epidermis of anaesthetized living hairless mouse (see Fig. 2). Because of the undulating characteristic of epidermal layers, the recorded spectral image sections consisted of keratinocytes associated to stratum basale and stratum spinosum. Note that only keratinocytes in the stratum basale were analyzed. We acquired images of basal cells since their keratin content is less than that of the other epidermal layers, thus minimizing keratin autofluorescence contribution to the overall emission spectrum. Bright green-fluorescing hair follicles were also observed in the spectral images (see Fig. 2, *red arrows*). The mice were subjected to total acute ischemia during which the intrinsic fluorescence of the keratinocytes increased in intensity by an average of 71 ± 5% (averaged from t = 50 min to t = 80 min) as depicted in Fig. 3, *A* and *B*. At t > 80 min, a decrease in autofluorescence intensity was observed to below pre-ischemic baseline or normoxic levels. The autofluorescence of the hair follicles remained fairly constant (± 4%) throughout the experiment. The variation in the cellular autofluorescence emission spectral shape after the onset of ischemia is depicted in Fig. 3, *A* and *C*. The spectra showed an initial blue-shift of the spectral peak from 456 nm (t = 0 min) to 450 nm (t = 20 min) and a subsequent red-shift to 455 nm (t = 80 min). At t = 150 min, the autofluorescence spectral peak was observed to be 460 nm, 5 nm longer than the normoxic (t = 0 min) autofluorescence spectrum. The variation in the spectral shape as demonstrated by the shifting of the spectral peaks strongly indicates metabolic response to ischemia of at least two spectral components. The difference spectra, that is the difference between the autofluorescence spectrum at any given time point (ischemic) and the baseline (normoxic) autofluorescence spectrum at t = 0 min, showed a more clear evidence that at least two components with different response to ischemia comprise the cellular autofluorescence spectrum (see Fig. 3 *D*). Here, it can be deduced that during the early condition after the onset

of ischemia, the intensity of short-wavelength spectral component increased more than the long-wavelength spectral component. At ~80 min, both components have higher intensities relative to normoxic levels but of relatively equivalent ratio as that of the normoxic condition. At longer times, both components decreased in intensity below the normoxic level as depicted by negative values in the difference spectrum for $t > 110$ min (see Fig. 3 D).
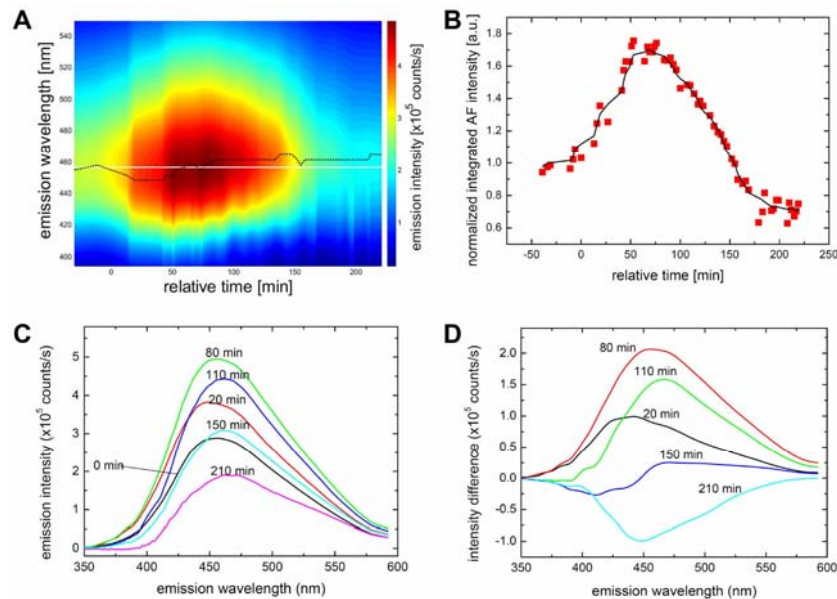

Fig. 3. *A:* Color map of the temporal behavior of the autofluorescence spectra obtained from the pixel-averaged spectral data from a region of interest (ROI; yellow box in Fig. 2). White line indicates the average peak wavelength ($\lambda = 456$ nm) of the autofluorescence spectra before ischemia. Black dotted line indicates the autofluorescence peak wavelength depicting spectral blue-shift after ischemia ($t > 0$ min) and a red-shift at $t > 50$ min. *B*: Normalized integrated autofluorescence intensity (integrated between 400 nm and 600 nm). *C*: ROI pixel-averaged autofluorescence spectra at representative time points showing spectral variation during ischemia. *D*: Difference spectra (relative to AF spectrum at $t = 0$ min) at representative time points.

3.2. Probing bound/free NADH in mouse keratinocytes

To observe the dynamics of cellular components related to metabolic cycle following ischemia, linear spectral unmixing of the pixel-averaged spectra was carried out. Globally fitting the difference spectra at all time points after the onset of ischemia ($t > 0$ min) in wavenumber space with model Gaussian curves yielded three spectral components with peak/full-width-at-half-maximum (FWHM) values of: 448 nm/ 91 nm; 459 nm/ 91 nm and; 528 nm/ 77 nm (see Fig. 4 *A*). Shown in Fig. 4 *B*, is an example of the fitting of the three components depicting a good fit of the sum of the fit to the data with typical fitting r^2 coefficient of determination of >0.99. Note also that the third spectrum has a minimal contribution to the overall spectrum. To validate the results of the global fitting procedure (i.e. peak wavelength of the spectral components), we plotted the χ^2 (global fitting) error as a function of the peak wavelengths of the components 1 and 2 as illustrated in Fig. 4, *C–E*. Here, the local minimum corresponds to peak wavelength values of 448 nm and 459 nm. These peak wavelengths as well as the spectral widths are in good agreement with literature values for protein-bound and free NADH [23,24].

The time-dependence of the amplitudes of the three spectral components for two independent *in vivo* experiment sets are shown in Fig. 5, *A* and *B*. Spectral unmixing revealed that indeed the third spectral component with amplitude A_3, attributed to flavin
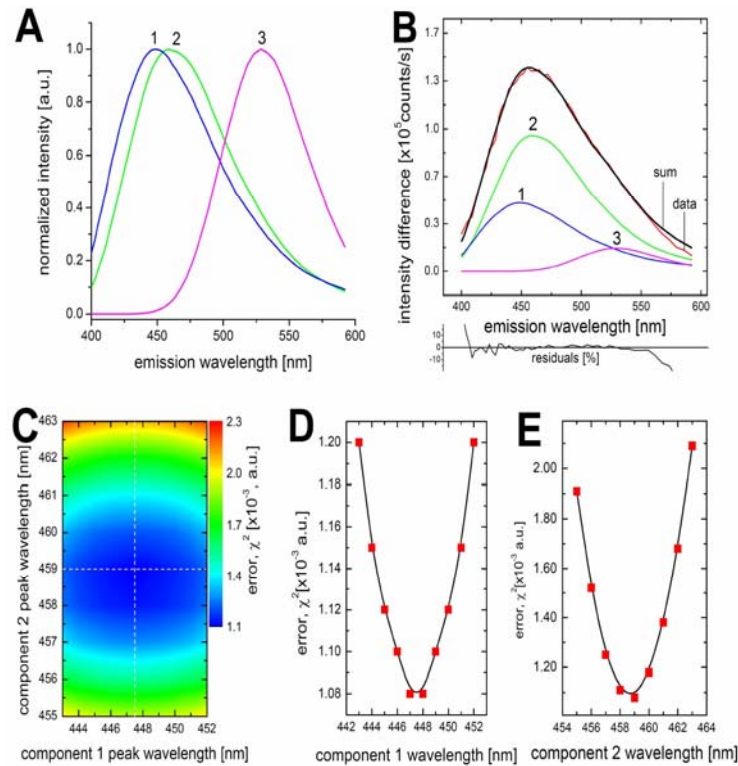
Fig. 4. *A*: Three spectral components used for spectral unmixing with peak/ full-width-at-half-maximum (FWHM) values of: (*1*) 448 nm/ 91 nm; (*2*) 459 nm/ 91 nm; and (*3*) 528 nm /77 nm, attributed to protein-bound and free NADH and flavins, respectively. Curves are normalized to the peaks' amplitude. *B*: Spectral unmixing analysis showing the spectral components (*1* to *3*) attributed to: (*1*) protein-bound NADH; (*2*) free NADH; and (*3*) flavins, and the sum of the fitted components. Also shown is the residual of the fit. Fitting r^2 coefficient of determination is 0.996. *C*: Color map of the χ^2 error obtained by global fitting ten arbitrary difference spectra as a function of the peak wavelengths of the first two components. The intersection point of the two dotted lines indicates the local minimum ($\lambda_1 = 448$ nm, $\lambda_2 = 459$ nm). *D* and *E*: Dependence of the global fitting error to the peak wavelength of spectral component 1 (at $\lambda_2 = 459$ nm) and peak wavelength of spectral component 2 (at $\lambda_1 = 448$ nm), respectively.
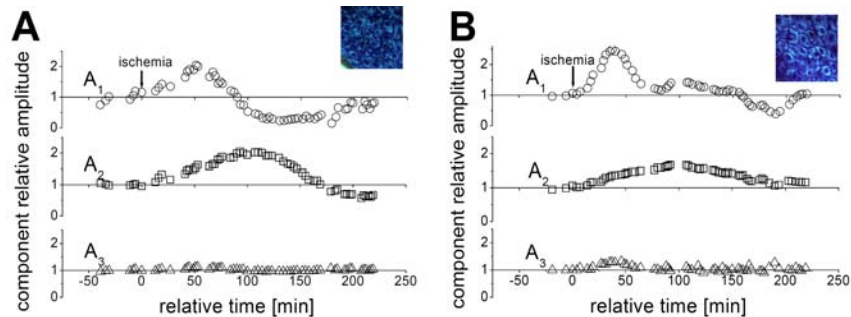

Fig. 5. *A* and *B:* Time-dependence of the relative amplitudes relative to the average component amplitudes at $t < 0$ min (normoxic) of each of the fitted components from two independent *in vivo* experiment sets. A minimum of 25 epidermal cells (within the region of interest as depicted in Fig. 2, *yellow box*), was measured for each time point, for each experiment. Reference (normoxic) condition ($t \leq 0$ min), ischemia ($t > 0$ min).

autofluorescence, has a minor contribution (~5%) to the overall spectral emission. Both experiments showed a significant difference between the amplitude variation of the two spectral components A_1 and A_2, attributed to protein-bound and free NADH fluorescence, respectively. Furthermore, similarities were found between the amplitude variations of corresponding spectral components. For instance, in both experiments, A_2 showed a broad peak in time (FWHM, ~100 min) with maxima at ~100 min while A_1 demonstrated a relatively narrower peak in time (FWHM, ~50 min) with maxima at ~50 min. These suggest that at early times following ischemia onset, the increase in fluorescence is mainly due to increase in protein-bound NADH (113%) and after $t = 50$ min, the protein-bound NADH autofluorescence decreases below normoxic levels (~70%) while free NADH remained increasing (up to ~85%). After ~100 min, free NADH gradually decreases below normoxic levels (~20%).
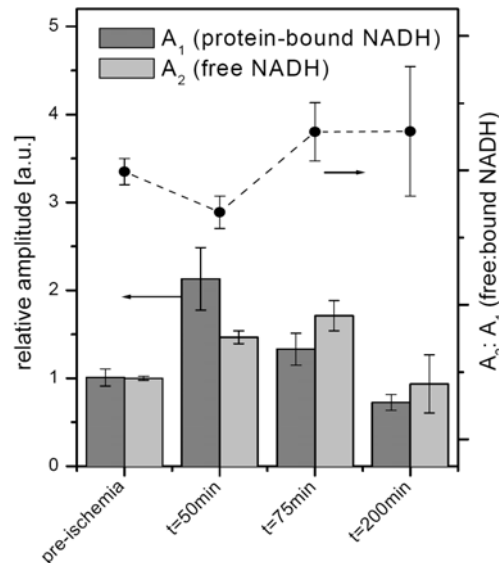

Fig. 6. *Left axis*: Shown are the amplitudes of the spectral components A_1 and A_2 attributed to protein-bound and free NADH, respectively, normalized to the average pre-ischemic values. *Right axis*: Relative ratio between the amplitudes of the two spectral components A_2 and A_1, attributed to free and protein-bound NADH, respectively.

The relative amplitudes (relative to the average component amplitudes at $t<0$) and the relative ratio of the two spectral components attributed to protein-bound and free NADH are shown in Fig. 6. Here, the results show that at early times after the onset of ischemia, the contributions of both protein-bound and free NADH increases but with higher increase in the contribution of the protein-bound. The increase in NADH autofluorescence following ischemia onset is an indication of the shift in the cellular redox state to a more reduced state. Ischemia results in complete glucose and oxygen deprivation (hypoxia followed by anoxia) and the absence of oxygen is known to inhibit oxidative phosphorylation. It has been shown that inhibition of oxidative phosphorylation (in this specific case by a mitochondrial complex 1 inhibitor) is accompanied by a significant increase in cellular protein-bound NADH fluorescence [8]. This might be related to the results of a study showing that binding of NADH to complex I enhances the fluorescence by 10-fold compared to only a 1.5 to 2-fold enhancement when they are bound to other sites including alcohol dehydrogenase, aldehyde dehydrogenase, glutamate dehydrogenase, malate dehydrogenase, lactate dehydrogenase, succinate dehydrogenase and citrate synthase [25]. Hypoxia results in the accumulation of NADH in complex I leading to a strong increase in the protein-bound NADH fluorescence, as observed here. This result is in agreement with the previous results on isolated hepatocytes in which a maximum value of the ratio bound:free NADH was observed at ~70 min after

exposure to hypoxia . After ~50 min, a sharp decrease in protein-bound NADH contribution was observed while the free NADH contribution remained increasing. A reasonable explanation is anoxia-mediated mitochondrial damage and subsequent autophagy [9]. This inhibition of mitochondrial ATP production results in the increased production of ATP by glycolysis and lactate fermentation (anaerobic metabolism). This shift in metabolic pathway results in a redistribution of protein-bound NADH to enzyme binding sites with shorter lifetimes (lower fluorescence quantum yield) [7,13], such as lactate dehydrogenase. Increased glycolysis is also observed in (pre)tumor cells (Warburg effect) and it has been reported that in such cells, increased levels of free NADH fluorescence are observed [6]. The duration in which the cell relies on glycolysis for ATP production depends on the amount of glucose in the tissue and the glucose uptake rate. The slow decrease in NADH autofluorescence after ~100 min is therefore most likely due to glucose deprivation [26].

4. Discussion

The results presented in this work demonstrate the dynamic effect of total acute ischemia on the autofluorescence spectra of *in vivo* mouse skin keratinocytes. Linear spectral unmixing analysis suggests that the metabolically active fluorophores are protein-bound and free NADH. The contributions of protein-bound and free NADH show different dynamic reactions to hypoxia, anoxia and ischemia. NADH protein-bound to the complex I (NADH:ubiquinone oxidoreductase) of mitochondria is the major source of protein-bound NADH fluorescence. The temporal protein-bound NADH profile shows the dynamics of the transition of normoxia to hypoxia to anoxia. The ratio between protein-bound and free NADH change when the cells shift to anaerobic metabolism and finally the deprivation of glucose reduces the total NADH fluorescence. Our results, therefore, signify that in mouse keratinocytes all the major metabolic pathways (glycolysis, anaerobic fermentation and oxidative phosphorylation) respond to the loss of blood-supplied (via capillaries) oxygen and glucose. Another important implication of our results is the confirmation of the presence of metabolically functional mitochondria in epidermal keratinocytes, contrary to the conclusion of a recent study that keratinocytes are functionally anaerobic and that keratinocytic mitochondria are metabolically dysfunctional [27]. Our observation showing significant response of mitochondrial-bound NADH to ischemia strongly suggests inhibition of mitochondrial complex I, hence, an evidence of mitochondrial oxidative phosphorylation of keratinocytes under normoxic conditions.

The results also demonstrate that although there is evidence supporting the hypothesis that cutaneous uptake of atmospheric oxygen contributes significantly to the oxygen supply of epidermis [28], capillary oxygen supply remains to be the major source for epidermal metabolic function. Based on optical measurements of oxygen flux on the surface of human skin, measured values of oxygen diffusion in skin tissues, and assumption of homogeneity of skin, the thickness of the skin tissue that is supplied by atmospheric oxygen was estimated to be 266–375 μm [28]. The measurements presented in the present study were carried out at depths of ~50 μm relative to the surface of the skin and the analysis of the results clearly showed metabolic response to complete deprivation of blood-supplied oxygen. On the other hand, the possibility that obstruction of blood supply establishes a hypoxic rather than an anoxic environment cannot be disregarded. In fact, it may even explain the slow metabolic response (~2 h) of the keratinocytes following the loss of blood-supplied oxygen.

The interpretation of the results of this study relies significantly on the validity of the spectral unmixing procedure which included fitting of the spectra with mathematically-modeled Gaussians as reference spectra. Although the Gaussian components do not exactly represent the spectra of pure compounds, the results strongly suggest that these fitted components are convenient representations of protein-bound and free NADH. On the other hand, the use of spectra of pure compounds as reference spectra in spectral unmixing will not yield more accurate results since the measured emission spectra are modulated by tissue inner filter effects (*i.e.*, light scattering and absorption in turbid media), tissue viscosity, refractive index and solvent effects [5,24,29]. Furthermore, the experiments were necessarily carried out

under anesthesia, and thus some level of anesthesia-related change particularly in the normoxic condition could influence the dynamic metabolic response of epidermal keratinocytes. A recent report showed a small change (<9%) in skin oxygenation of mice after one hour of administration of ketamine anesthesia under normoxic conditions [30].

Most imaging experiments on free and protein-bound NADH were carried out using two-photon excited fluorescence lifetime imaging (FLIM) [8–13]. Discrimination between the free and protein-bound NADH is achieved by taking advantage of the difference in their fluorescence lifetimes: the short lifetime component is attributed to the free NADH ($\tau_{freeNADH}$ = 0.3 to 0.5 ns) while the long lifetime component is attributed to the protein-bound NADH ($\tau_{boundNADH}$ = 1.6 to 3.7 ns) [8,9,12]. Comparison between FLIM and spectral imaging in terms of ability to discriminate between protein-bound and free NADH is not straightforward and depending on the type of experiment different aspects need to be taken into account. An important factor in the in-vivo imaging of NADH is the sensitivity and non-invasiveness of the applied method: autofluorescence levels are in general low and in in-vivo experiments only low excitation levels are tolerated. The high time resolution of FLIM dictates the use of photomultiplier tubes or avalanche photo diodes with peak quantum efficiencies in the range of 10-40% while the present spectral imaging setup is equipped with a detector with a >90% peak quantum efficiency. Moreover, FLIM requires the use of band-pass filters to select the emission of the NADH and suppress autofluorescence contributions from other components such as flavins. In contrast, spectral imaging detects a broad spectral range covering the entire (protein-bound and free) NADH emission band. In our experience both techniques require comparable amounts of signal for reliable analyses of the protein-bound and free NADH components. The higher sensitivity of spectral imaging results in discrimination between the two components at relatively short pixel dwell times of 2 ms per pixel compared to 11 to 17 ms per pixel [9–12] in FLIM studies. Furthermore, the spectral imaging provides valuable additional information on morphology and the presence of other components besides NADH.

Finally, this study has demonstrated the capability of nonlinear spectral metabolic imaging in obtaining both morphological and biochemical information to unravel the dynamic metabolic response of living cells inside tissues for a long period of time following acute ischemia. Our results represent clear indication that spectral imaging effectively discriminates protein-bound and free NADH.

Acknowledgments